

ADAPTIVE CONTROL OF AEROELASTIC SYSTEMS: AN IMMERSION AND INVARIANCE APPROACH

Andrea Mannarino^{*,†}, Paolo Mantegazza^{**,†}

* Ph.D. student, ** Professor

[†]Politecnico di Milano, Dipartimento di Scienze e Tecnologie Aerospaziali,
Via La Masa 34, 20156 Milano, Italy.

Corresponding author: andrea.mannarino@polimi.it

Keywords: *Nonlinear aeroservoelasticity, Immersion and Invariance control, Sliding mode observers.*

Abstract

The active suppression of aeroelastic limit cycle flutter oscillations is the main goal of this work. Because of the significant dependence of such outcomes upon flight conditions, an adaptive controller is selected. The related task is accomplished through a full state Immersion and Invariance feedback, embodying linear filters to simplify its design. A practical implementation is then obtained through a sliding mode observer reconstructing the required full state. The effect of different fidelities in the representation of the aerodynamic system will be verified for the classical test case of a typical section in transonic regime.

1 Introduction

The improvement of aircraft performances through active control systems is a well established research and industrial topic. As different sources state, the next generation of flight control systems will use adaptive and non-deterministic techniques to provide more stable and manoeuvrable airplanes [1].

Until the more recent decades, a somewhat inadequate computational power has restricted the routine study of aeroservoelastic systems to linear(ized) subsonic and supersonic flight regimes. Nowadays advances in com-

puter technology and Computational Fluid Dynamics (CFD) allow to accurately evaluate unsteady loads for inviscid and viscous flows in transonic regime. Therefore, the adoption of CFD-based aeroservoelastic analyses is becoming more and more viable [2], allowing studies of transonic flows with strong shocks, possibly characterized by large motion, whereas nonlinear phenomena, such as weak divergence and Limit Cycle Oscillations (LCOs) can occur. The full control of these dangerous events is of utmost importance in avoiding unacceptable vibrations, self-induced oscillations, ride-quality deterioration and fatigue failures [3].

In this work an Immersion and Invariance (I&I) approach [4–9] is employed to stabilize an aeroelastic system beyond the flutter bifurcation velocity. The related theory and a large number of applications to mechanical systems, including airplanes trajectory tracking, can be found in [4], while applications to spacecraft systems are addressed in [5]. The adoption of an I&I methodology for simple aeroelastic systems is considered in [7–9], where both single and multiple input, full state based control laws are studied.

Here active flutter suppression controllers will be designed on a realistic generic scheme of reduced order models, including sensors and actuators, which can be either linear or nonlinear, and then verified through higher fidelity simu-

lations characterized by a CFD-based representation of the aerodynamic system. Even if an I&I observer formulation could be devised [4], a simpler, more agile and robust, nonlinear sliding mode estimation of the required system state will be preferred for a practical implementation of a full state I&I controller.

The whole design procedure will be verified on the control of a simple pitching and plunging typical section, featuring a NACA 64A010 airfoil. This case is characterized by highly nonlinear unsteady aerodynamic loads, producing large shock motions and allows to verify the importance of including the dynamics of sensors and actuators, resulting so in a challenging test for the proposed approach.

2 Aeroservoelastic models

An aeroservoelastic system is typically composed by three interconnected parts: structure, aerodynamics and control, and, depending on specific analysis and design needs, different model fidelities can be used in the various stages of its development. Here we give an introduction to the modeling of each sub-system.

2.1 Structural dynamics model

Following a standard approach, a generic linear(ized) structural model, can be discretized into the classical multi-degrees of freedom scheme:

$$\mathbf{M}_s \ddot{\mathbf{q}}_s + \mathbf{C}_s \dot{\mathbf{q}}_s + \mathbf{K}_s \mathbf{q}_s = q_\infty \mathbf{f}_a + \mathbf{T}_\beta^T \mathbf{m}_\beta \quad (1)$$

where: \mathbf{M}_s , \mathbf{C}_s , \mathbf{K}_s are the structural mass, damping and stiffness matrices, \mathbf{q}_s the generalized structural coordinates, whose physical meaning is determined by the assumed discretization and \mathbf{f}_a the external generalized aerodynamic forces, scaled by the asymptotic dynamic pressure q_∞ .

To explain the term $\mathbf{T}_\beta^T \mathbf{m}_\beta$ in the above formula, it is remarked that the driving degree of freedom of any control surface is typically embedded in \mathbf{q}_s , so to be easily interfaced to the aerodynamic subsystem in the very same way as any other structural motion. Therefore, control surface rotations, β , will be defined by $\beta = \mathbf{T}_\beta \mathbf{q}_s$, \mathbf{T}_β being an appropriate linking kinematic matrix, so that the generalized hinge moments, \mathbf{m}_h ,

associated to the external control moments, \mathbf{m}_β , will be given by $\mathbf{m}_h = \mathbf{T}_\beta^T \mathbf{m}_\beta$.

In the case of a typical section, the matrices of Eq. 1 are so composed:

$$\begin{aligned} \mathbf{q}_s &= \{h \quad \theta \quad \beta\}^T \\ \mathbf{M}_s &= \begin{bmatrix} m & S_{h\theta} & S_{h\beta} \\ S_{h\theta} & J_{\theta\theta} & 0 \\ S_{h\beta} & 0 & J_{\beta\beta} \end{bmatrix} \\ \mathbf{C}_s &= \begin{bmatrix} 2\xi_m \omega_{hh} & 0 & 0 \\ 0 & 2\xi J_{\theta\theta} \omega_{\theta\theta} & 0 \\ 0 & 0 & 0 \end{bmatrix} \\ \mathbf{K}_s &= \begin{bmatrix} m\omega_{hh}^2 & 0 & 0 \\ 0 & J_{\theta\theta} \omega_{\theta\theta}^2 & 0 \\ 0 & 0 & 0 \end{bmatrix} \end{aligned} \quad (2)$$

2.2 Actuator and sensor models

After defining with $\mathcal{D}(\mathbf{v})$ the diagonal matrix associated to a vector \mathbf{v} , we assume that a set of position servos, commanding β to β_c , can be adequately modeled as:

$$\begin{aligned} \ddot{\mathbf{x}}_{\text{act}} + \mathcal{D}(2\xi_{\text{act}} \omega_{\text{act}}) \dot{\mathbf{x}}_{\text{act}} + \mathcal{D}(\omega_{\text{act}}^2) \mathbf{x}_{\text{act}} &= \mathcal{D}(\omega_{\text{act}}^2) \beta_c \\ \mathbf{m}_\beta &= \mathcal{D}(\mathbf{k}_\beta) (\mathbf{x}_{\text{act}} - \mathbf{T}_\beta \mathbf{q}_s) \\ |\mathbf{x}_{\text{act}}| \leq \mathbf{x}_{\text{act,max}}, |\dot{\mathbf{x}}_{\text{act}}| \leq \dot{\mathbf{x}}_{\text{act,max}}, |\mathbf{m}_\beta| \leq \mathbf{m}_{\beta,\text{max}} \end{aligned} \quad (3)$$

with ξ_{act} and ω_{act}^2 defining the actuator bandwidth, \mathbf{k}_β an assumed acceptable low frequency residualization of their dynamic compliance, the 'max' suffixed terms indicating the related (symmetric) saturation values. Furthermore, in view of the need of modeling only the transfer function of accelerometer based measures, the related output, at assigned locations, will be given by $\mathbf{a} = \mathbf{T}_a \ddot{\mathbf{q}}_s$, \mathbf{T}_a being a suitable displacement interpolation matrix. Therefore, the related transducer dynamics (sensor, compensation, antialiasing filter) is approximated through:

$$\ddot{\mathbf{x}}_s + \mathcal{D}(2\xi_s \omega_s) \dot{\mathbf{x}}_s + \mathcal{D}(\omega_s^2) \mathbf{x}_s = \mathcal{D}(\omega_s^2) \mathbf{T}_a \ddot{\mathbf{q}}_s \quad (4)$$

2.3 Aerodynamic models

Taking for granted its stability, a generic formulation of a nonlinear unsteady aerodynamic system is written as:

$$\begin{cases} \dot{\mathbf{x}}_a &= \mathbf{f}_{x_a}(\mathbf{x}_a, \mathbf{q}_s, \dot{\mathbf{q}}_s) \\ \mathbf{f}_a &= \mathbf{f}_a(\mathbf{x}_a, \mathbf{q}_s, \dot{\mathbf{q}}_s) \end{cases} \quad (5)$$

where \mathbf{x}_a is the aerodynamic state, which can be either a physical entity, as in the case of a raw CFD model, or a generically abstract reduced order state, as detailed in the following.

2.3.1 CFD modeling

The aerodynamic sub-system is modeled by a cell centered Finite-Volume (FV) scheme, using the aerodynamic code **AeroFoam**, developed at Dipartimento di Scienze e Tecnologie Aerospaziali, Politecnico di Milano [10]. **AeroFoam** is a density-based compressible Unsteady Euler/Reynolds-Averaged-Navier-Stokes (URANS) solver, with the Euler option being selected in this work. Among its features there is an aeroelastic interfacing scheme, based on a Moving Least Squares (MLS) interpolation strategy, providing all the needed functionalities to set the appropriate aerodynamic boundary conditions imposed by a deforming structure, while driving a connected hierarchical mesh deformation within an Arbitrary Lagrangian Eulerian (ALE) formulation. An extended illustration of its aeroelastic capabilities can be found in [10]. In this work any of **AeroFoam** aerodynamic formulations can be synthesized in the form of Eq. 5, with \mathbf{x}_a being the physical state associated to the FV cell centers, i.e. density, momentum, energy and the turbulence model own state. The generalized aerodynamic loads are computed through the integration of the pressure and viscous stresses on the body surface. The high number of states (from tens of thousands to millions) required for an accurate approximation implies highly time demanding CFD-based analyses. Consequently, such simulations are mostly restricted to the verification phases of a design.

2.3.2 Reduced order modeling

For classical linear(ized) flows, mostly based on the solution of an integral equation, linear identification methods can be exploited to provide a reduced order state space representation, see [11] and references therein. Even when the flow is nonlinear, e.g. Euler-based CFD codes, linear load identification methods can be adopted for small motions around a steady trimmed so-

lution [12]. Nevertheless, when the structural system undergoes large enough motions, causing significant changes of the flow field, e.g. moving shocks, an unsteady, nonlinear aerodynamic model of the type previously described is required. As already remarked, it can provide a high level of fidelity only at the cost of a significantly fine discretization, with the related demand of computational power and time consuming simulations. This fact limits its applicability to control designs, sensitivity studies and system optimization, for which a Reduced Order Model (ROM) is almost compulsory [13]. Different approaches for the determination of nonlinear aerodynamic ROMs are available in the literature [12, 13].

In this work it has been chosen to exploit a continuous time recurrent neural network [14] to compactly identify the unsteady, nonlinear relation between the structural motion and the aerodynamic loads. After defining the structural dynamics state as $\mathbf{x}_s = [\mathbf{q}_s \ \dot{\mathbf{q}}_s]^T$, the related stable aerodynamic ROM can be appropriately defined with the following set of ordinary differential equations:

$$\begin{cases} \dot{\mathbf{x}}_a &= \mathbf{A}_r \phi(\mathbf{x}_a) + \mathbf{B}_r \mathbf{x}_s \\ \mathbf{f}_a &= \mathbf{C}_r \phi(\mathbf{x}_a) + \mathbf{D}_r \mathbf{x}_s \end{cases} \quad (6)$$

where $\phi : \mathbb{R}^{N_a} \rightarrow \mathbb{R}^{N_a}$ is a function vector whose elements are hyperbolic tangent functions, i.e. $\phi_i(x) = \tanh x$. The matrices \mathbf{A}_r , \mathbf{B}_r , \mathbf{C}_r , \mathbf{D}_r contain the network synaptic weights, which are tuned through a two-levels training procedure based on optimization schemes. The first level, which initializes the coefficients, is based on a Genetic Algorithm minimizing a quadratic cost function of the output error: $F = \frac{1}{2} \sum_{i=1}^{N_t} \|\mathbf{f}_{a,ROM}(t_i) - \mathbf{f}_{a,CFD}(t_i)\|^2$, where N_t is the number of training samples considered. A good compromise between an acceptable accuracy at the end of this phase and its computational time can be achieved by setting the probability of mutation approximately at 0.15, along with a maximum of 150 generations allowed. Then, starting from the best population resulting from the initialization phase, the second training level exploits the Levenberg-Marquardt algorithm, based

on the same cost function, eventually driving the identification error to a desired converged precision at a faster pace.

The training signals are generated within the previously described CFD solver. Random signals are given in input to all the structural degrees of freedom simultaneously. Amplitude and frequency ranges to be excited are chosen by running a few open loop CFD-based aeroelastic simulations.

2.4 Complete aeroservoelastic model

Defining the extended servo-elasto-mechanical degrees of freedom $\mathbf{q} = [\mathbf{q}_s \ \mathbf{x}_{\text{act}} \ \mathbf{x}_s]^T$ and the corresponding state $\mathbf{x} = [\mathbf{q} \ \dot{\mathbf{q}}]^T$, putting together all of what above, we are led to the following non-linear, strictly proper, state space formulation:

$$\begin{cases} \dot{\mathbf{x}} &= \mathbf{A}\mathbf{x} + \mathbf{B}_c\beta_c + q_\infty\mathbf{B}_a\mathbf{f}_a(\mathbf{x}_a, \mathbf{q}_s, \dot{\mathbf{q}}_s) + \mathbf{B}_s\mathbf{u}_{\text{sat}} \\ \dot{\mathbf{x}}_a &= \mathbf{f}_{x_a}(\mathbf{x}_a, \mathbf{q}_s, \dot{\mathbf{q}}_s) \\ \mathbf{y} &= \mathbf{C}_y\mathbf{x} \end{cases} \quad (7)$$

where \mathbf{y} is a measure output, while \mathbf{u}_{sat} contains the actuator saturation effects detailed in Eq. 3.

3 Control methodology

3.1 Immersion and Invariance adaptive controller

Controllers based on the Immersion and Invariance (I&I) into stable manifolds are a somewhat novel concept. The related theory can be found in [4], while some applications to aeroelastic systems are reported in [7–9]. The filter embedment approach adopted here can be found in [5,6]. The basic I&I idea is to achieve a stabilisation by immersing the plant dynamics into a stable target system, possibly described by a reduced number of states. Then, by introducing appropriate adaptive terms in the related controller, it is possible to achieve the invariance of the manifold containing such a target [4].

In this work the target system is represented by:

$$s = \dot{\tilde{y}} + \lambda\tilde{y} \quad (8)$$

λ being a positive tunable design parameter and \tilde{y} the controlled target performance, which can be

any linear combination of the system state components. Anticipating that only the displacement at a key point of the structure will be taken into account, we can write:

$$\tilde{y} = \mathbf{H}\mathbf{x} = [\mathbf{H}_q \ \mathbf{0}] \begin{Bmatrix} \mathbf{q} \\ \dot{\mathbf{q}} \end{Bmatrix} = \mathbf{H}_q\mathbf{q} \quad (9)$$

with \mathbf{H} and \mathbf{H}_q defining the appropriate single line target output matrix, specified on a case by case basis to define the desired \tilde{y} . It must be remarked that, since we aim at a stabilization through a single control input, a multi-components target will result in a singular controller. It would nevertheless be possible to take into account any additional performance of interest, but, as shown in [9], the number of control input must be increased accordingly. Since the performance dynamics must be asymptotically stable over the manifold $s = 0$, it is sufficient to develop a control law driving s to the origin. By differentiating Eq. 8, the dynamics of s is driven by the following equation:

$$\dot{s} = \ddot{\tilde{y}} + \lambda\dot{\tilde{y}} \quad (10)$$

where the required \tilde{y} derivatives are explicitly defined through:

$$\begin{aligned} \dot{\tilde{y}} &= \mathbf{H}\mathbf{A}\mathbf{x} = \mathbf{H}_q\dot{\mathbf{q}} \\ \ddot{\tilde{y}} &= \mathbf{H}\mathbf{A}^2\mathbf{x} + q_\infty\mathbf{H}\mathbf{A}\mathbf{B}_a\mathbf{f}_a + \mathbf{H}\mathbf{A}\mathbf{B}_s\mathbf{u}_{\text{sat}} + \mathbf{H}\mathbf{A}\mathbf{B}_c\beta_c \end{aligned} \quad (11)$$

According to such results, Eq. 10 becomes:

$$\begin{aligned} \dot{s} &= \mathbf{H}\mathbf{A}^2\mathbf{x} + q_\infty\mathbf{H}\mathbf{A}\mathbf{B}_a\mathbf{f}_a + \mathbf{H}\mathbf{A}\mathbf{B}_s\mathbf{u}_{\text{sat}} + \mathbf{H}\mathbf{A}\mathbf{B}_c\beta_c + \lambda\mathbf{H}_q\dot{\mathbf{q}} \\ &= \mathbf{x}^T\boldsymbol{\alpha} + q_\infty\mathbf{f}_a^T\boldsymbol{\omega} + \mathbf{u}_{\text{sat}}^T\boldsymbol{\gamma} + b\beta_c + \lambda\mathbf{H}_q\dot{\mathbf{q}} \end{aligned} \quad (12)$$

with: $\boldsymbol{\alpha} = (\mathbf{H}\mathbf{A}^2)^T$, $\boldsymbol{\omega} = (\mathbf{H}\mathbf{A}\mathbf{B}_a)^T$, $\boldsymbol{\gamma} = (\mathbf{H}\mathbf{A}\mathbf{B}_s)^T$ and $b = \mathbf{H}\mathbf{A}\mathbf{B}_c$, being unknown constant parameters, except for the sign of b , which is assumed as known. Then, after defining the positive design parameter c_s , an asymptotically stable manifold is enforced by adding and subtracting the term $c_s s$ to Eq. 10, obtaining:

$$\dot{s} = \mathbf{x}^T\boldsymbol{\alpha} + q_\infty\mathbf{f}_a^T\boldsymbol{\omega} + \mathbf{u}_{\text{sat}}^T\boldsymbol{\gamma} + b\beta_c + \lambda\mathbf{H}_q\dot{\mathbf{q}} + c_s s - c_s s \quad (13)$$

After defining the following vectors:

$$\begin{aligned} \hat{\boldsymbol{\chi}} &= [b^{-1}\boldsymbol{\alpha} \ b^{-1}\boldsymbol{\omega} \ b^{-1}\boldsymbol{\gamma} \ b^{-1}]^T \\ \boldsymbol{\Psi} &= [\mathbf{x} \ q_\infty\mathbf{f}_a(\mathbf{x}_a, \mathbf{q}_s, \dot{\mathbf{q}}_s) \ \mathbf{u}_{\text{sat}} \ (\lambda\mathbf{H}_q\dot{\mathbf{q}} + c_s s)]^T \end{aligned} \quad (14)$$

Eq. 13 can be written in the following compact form:

$$\dot{s} = -c_s s + b(\beta_c + \Psi^T \hat{\chi}) \quad (15)$$

In order to somewhat simplify the I&I design procedure presented in Ref. [4], $s = \mathbf{H}_q(\dot{\mathbf{q}} + \lambda \mathbf{q})$, Ψ and β_c are low pass filtered and attenuated [5,6,8] in accordance with the following equations:

$$\dot{s}_f = -\mu s_f + \mathbf{H}_q(\dot{\mathbf{q}} + \lambda \mathbf{q}) \quad (16a)$$

$$\dot{\Psi}_f = -\mu \Psi_f + \Psi \quad (16b)$$

$$\dot{\beta}_{c,f} = -\mu \beta_{c,f} + \beta_c \quad (16c)$$

where μ is a further positive design parameter. Given that the proposed linear filters are asymptotically stable, it can be shown [8] that the following ordinary differential equation is satisfied asymptotically:

$$\dot{s}_f = -c_s s_f + b(\beta_{c,f} + \Psi_f^T \hat{\chi}) \quad (17)$$

Since $\hat{\chi}$ is unknown, I&I approximates it through the aid of shaping terms which will force the stable manifold to be invariant. Within such a view, we define the off-the-manifold variable \mathbf{z} [4]:

$$\mathbf{z} = (\chi + \delta) - \hat{\chi} \quad (18)$$

with $\delta(s_f, \Psi_f)$ being a yet to be chosen shaping function, so that, defining a control law of the form $\beta_{c,f} = -\Psi_f^T(\mathbf{z} + \hat{\chi})$, it is possible to cancel the unknown constant parameter vector $\hat{\chi}$ of Eq. 17, which becomes:

$$\dot{s}_f = -c_s s_f - b \Psi_f^T \mathbf{z} \quad (19)$$

Using Eq. 16c we can write our control law $\beta_c = \mu \beta_{c,f} + \dot{\beta}_{c,f}$ as:

$$\beta_c = -\Psi^T(\chi + \delta) - \Psi_f^T(\dot{\chi} + \dot{\delta}) \quad (20)$$

Following the procedure presented in [7, 8], it can be proved that the following shaping function makes the \mathbf{z} -dynamics asymptotically stable:

$$\delta = \gamma_{\text{Con}} \text{sign}(b) s_f \Psi_f \quad (21)$$

where γ_{Con} is an additional positive design constant. Combining all the previous definitions, we come up with the following adaptive law:

$$\begin{cases} \dot{s}_f &= -\mu s_f + \mathbf{H}_q(\dot{\mathbf{q}}_o + \lambda \mathbf{q}_o) \\ \dot{\Psi}_f &= -\mu \Psi_f + \Psi_o \\ \dot{\chi} &= \gamma_{\text{Con}} \text{sign}(b) s_f [-\Psi_o + \Psi_f(c_s + \mu)] \end{cases} \quad (22)$$

and the resulting control law:

$$\begin{aligned} \beta_c &= -\Psi^T(\chi + \delta) \\ &\quad - \gamma_{\text{Con}} \text{sign}(b) \Psi_f^T \Psi_f [\mathbf{H}_q(\dot{\mathbf{q}}_o + \lambda \mathbf{q}_o) + (c_s - \mu) s_f] \end{aligned} \quad (23)$$

where the suffix o indicates that the related quantities are computed using the state values that will be provided by the sliding observer described in the following paragraph.

3.2 Sliding mode observer

The previously described I&I controller requires the availability of the system state for its implementation. Since the significant differences between the design and verification models may cause system instabilities and performance degradation, it has then been decided to resort to a robust sliding mode observer. Thanks to its formulation, a separation principle can be exploited [15], so any observer-based implementation can be carried out without regard to the controller design. At first the method of reference [16] was successfully adopted. Nevertheless, while practicing with its design, it appeared that the resulting observer did not change significantly the aerodynamic eigenvalues, thus suggesting that the related reduced order aerodynamic state was more detectable than observable. So, after verifying that it provided equivalent results, a simpler scheme was chosen. It allows the direct use of an aerodynamic ROM without the need of any linearization and, recalling Eq. 7, has the form:

$$\begin{cases} \dot{\mathbf{x}}_o &= \mathbf{A} \mathbf{x}_o + \mathbf{L}_{\text{Obs}} \mathbf{e}_o + \mathbf{B}_c \beta_c + \\ &\quad q_\infty \mathbf{B}_a \mathbf{f}_{a,o} + \gamma_{\text{Obs}} \mathbf{v}_s \\ \dot{\mathbf{x}}_{a_o} &= \mathbf{f}_{x_a}(\mathbf{x}_{a_o}, \mathbf{q}_{s_o}, \dot{\mathbf{q}}_{s_o}) \end{cases} \quad (24)$$

where $\mathbf{e}_o = \mathbf{y} - \mathbf{C}_y \mathbf{x}_o$ is the output error, \mathbf{x}_o and \mathbf{x}_{a_o} are, respectively, the observed servo-elasto-

mechanical and aerodynamic state, with the observed structural generalized coordinates, \mathbf{q}_{s_o} and $\dot{\mathbf{q}}_{s_o}$, being just the related partitions of \mathbf{x}_o . Finally, \mathbf{v}_s is the sliding contribution, chosen as in [16], function of the output error \mathbf{e}_o .

4 Numerical results

This example has been chosen for two main reasons: it shows the ability of an I&I controller to stabilise the response of a significantly nonlinear system and demonstrates the importance of a correct modeling in the design phase. It is related to a plunging and pitching typical section, featuring a NACA 64A010 airfoil, with a trailing edge flap, schematically represented in Fig. 1, at sea level and $M_\infty = 0.8$, whose structural data can be found in [17, 18]. It is a kind of bench-

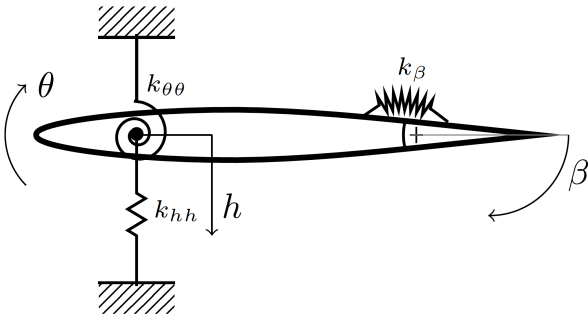
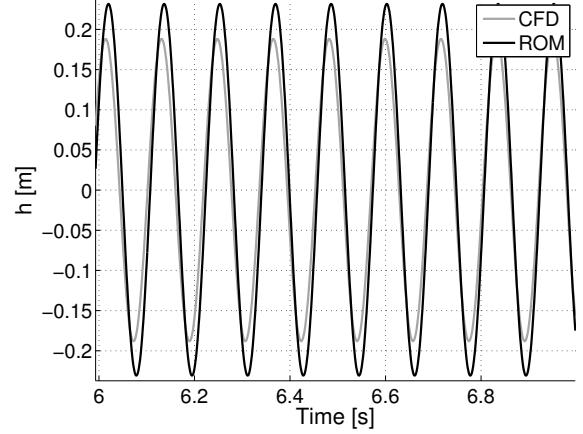


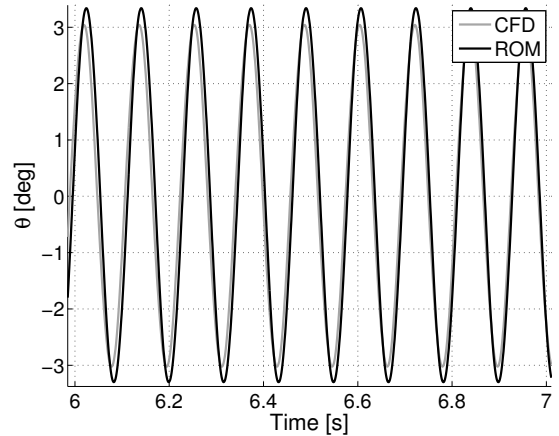
Fig. 1 : Typical section.

mark characterized by a significantly complex unsteady nonlinear aerodynamic behavior [17], producing ample limit cycles having a frequency in excess of 10 [Hz], which cannot be matched by an overly simplified aerodynamic approximation. For such a reason a reference high fidelity AeroFoam-Euler approximation of 12000 two dimensional cells, i.e. 48000 unknowns, will be used as the base for its validation. After remarking that the servo-elastic subsystem will add just 12 states (6-structural, 2-actuator and 4-sensors), it should be clear that the overall system size is dominated by a huge number of aerodynamic states, which is unsuitable for the design of any active controller. Using the reduced order model presented in Section 2.3.2, a number of 4 aerodynamic states has proven sufficient to reproduce sufficiently accurate aeroelastic responses in the

range of flight conditions of interest. A sample of the obtained open loop results is shown in Fig. 2. Running a few aeroelastic open loop simu-



(a) Plunge LCO response.



(b) Pitch LCO response.

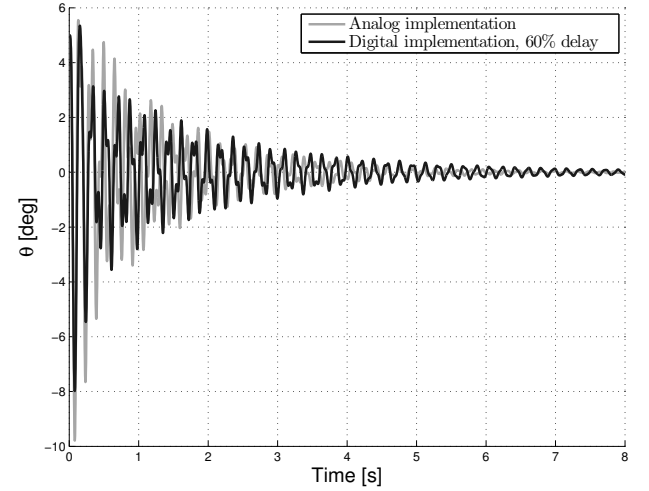
Fig. 2 : Comparison of CFD- and ROM-based aeroelastic LCO response, $V_\infty = 200$, m/s.

lations, we have found out that the system develops limit cycle solutions beyond the numerically estimated flutter velocity $V_{F,OL} = 193$, m/s. The actuator bandwidth has been set to 13, Hz, while two accelerometers with bandwidth of 30, Hz have been virtually placed at the leading edge and slightly before the flap hinge line, permitting a full state reconstruction by the observer. The equivalent stiffness of the control chain has been set to $k_\beta = 1.7 \cdot 10^4$, Nm. The actuator saturates at $\beta_{\max} = 10$, deg and $\dot{\beta}_{\max} = 40$, deg/s. To assure the system adaptivity and stability over a wide range of operating conditions, the con-

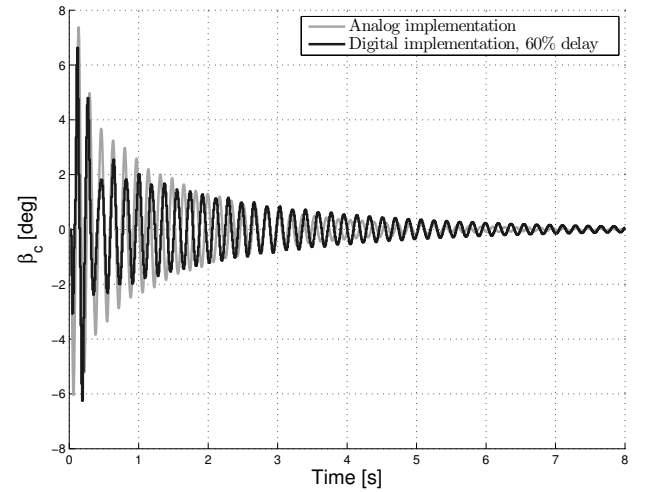
troller parameters are tuned considering various flight speed, at least 25% greater than the open loop linearized flutter speed, combined with different type of simulations, such as the response to large initial conditions, to input pulses, eventually evaluating the controller adaption speed when its compensator is switched off-on during a simulation. All the tuned designs and verifications have been determined by using an explicit Runge-Kutta integrator with adaptive step control, providing a precision adequate to allow an exact matching of saturation/desaturation time instants. Moreover a realistic digital implementation of the proposed controller has been taken into account. Through some preliminary continuous designs, it has been possible to verify that the sampled behavior of the continuous sliding observer and I&I compensator could be adequately matched at a frequency of 200, Hz, the related discretization being based on a fixed step Runge-Kutta-Heun integration scheme. A comparison between analogical and digital implementations can be better appreciated analyzing Fig. 3, where an additional, conservatively large, processing delay associated to the chosen data acquisition system and control computer has been taken into account, here expressed as a fraction of the related sampling time. We want to remark that a vast set of simulations has been carried out against: varied ROM and finely discretized aerodynamic models, system disturbances and measurement noise, a $\pm 20\%$ change of most of the structural parameters. Nevertheless, for sake of brevity, only samples of the related results will be presented, trying to blend them in a way providing as a complete as possible picture of some interesting findings of this work.

4.1 Control law design

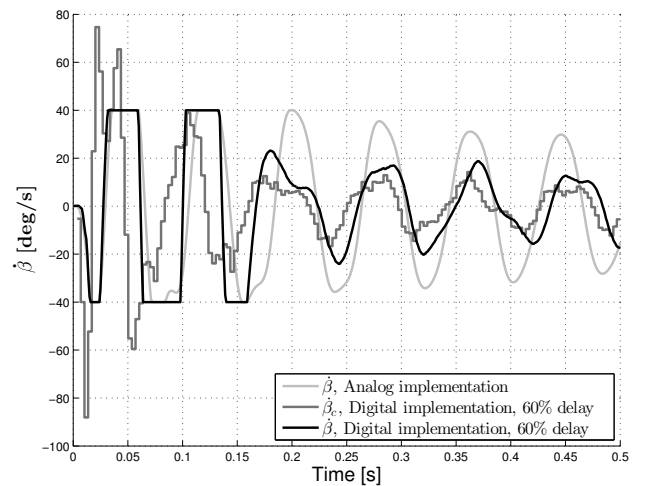
To achieve good adaptive performances against pulse perturbations applied through the flap, different flight speeds, up to 25% of $V_{F,OL}$, are taken into account to tune the controller parameters. The target performance, Eq. 9, is the (linearized) vertical displacement of the typical section leading edge, so that, being $\mathbf{q} = [h \ \theta \ \beta \ x_{act} \ x_{s1} \ x_{s2}]^T$ we have $\mathbf{H}_q =$



(a) Pitch response.



(b) Control surface deflection



(c) Control speed, with saturations.

Fig. 3 : Comparison of a continuous and digital controller implementation.

$[1 \ l_{LE} \ 0 \ 0 \ 0 \ 0]$, where l_{LE} is the distance between the elastic center of the airfoil and its leading edge. Carrying out the design with a trial and error-like procedure, the control parameters of Table 1 are obtained.

γ_{Obs}	0.5
λ	50
c_s	30
μ	750
γ_{Con}	0.05

Table 1: Controller parameters.

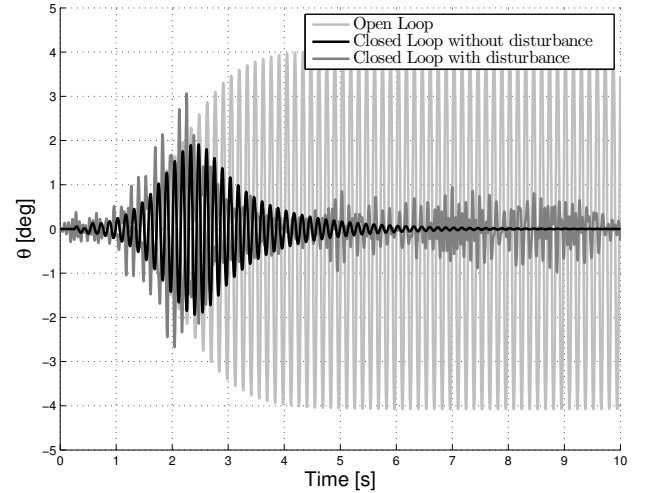
At first, Fig. 4 depicts a sample response of the controlled typical section to an input pulse applied at the design point. A significant random disturbance, having a maximum amplitude of 1.5, deg, has been applied to the control surface, so showing the controller insensitivity to disturbances.

4.2 Control law verification

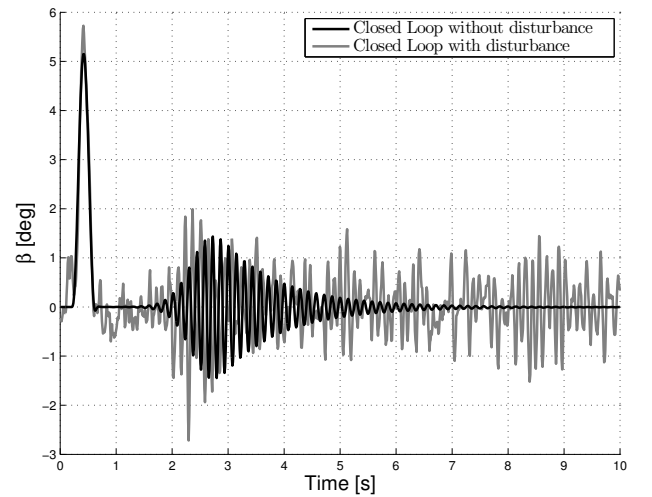
A few high fidelity responses at the off-design condition of $V_\infty = 255$, m/s are presented in Fig. 5, where the controller is switched on after 4 seconds, when the limit cycle is fully developed. Spillover effects over the larger aerodynamic model have not been found in any of the verifications carried out.

Some samples of the flow field during the limit cycle suppression are depicted in Fig. 6, showing a significant shock oscillation amplitudes of the order of 23% of the chord. The controller appropriately cancels the large disturbance command applied by the control, eventually driving such a amplitude down to 2% of the chord.

Nevertheless, despite the good outcomes obtained, it can be useful to remark that the robustness of an I&I controller can result in being inadequate against excessively simplified design models, e.g. unmodeled sensor and actuator dynamics. For example, if we totally neglect those dynamics, a design at $V_\infty = 211$ [m/s] will provide good performances with the parameters of Table 2, with a sample of the control surface rotation being depicted in Fig. 7a. Instead, by verify-



(a) Pitch response to input pulse.



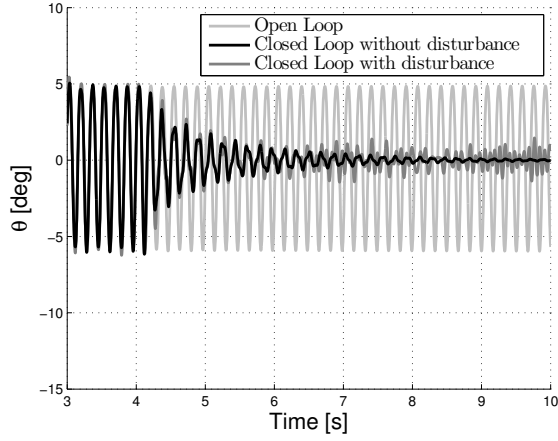
(b) Related control effort.

Fig. 4 : Input pulse response of the design model, $V_\infty = 211$, m/s.

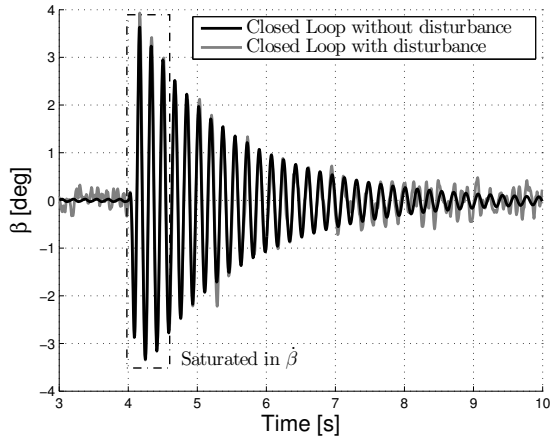
γ_{Obs}	0.5
λ	50
c_s	30
μ	125
γ_{Con}	0.1

Table 2: Controller parameters: ideal typical section, no sensor-actuator dynamics.

ing the very same controller after accounting for its digital implementation and the very same actuator adopted in the previous design, we can see, in Fig. 7b, that it results in a rather violent instability. As witnessed by Fig. 7c, something similar, albeit with a somewhat softer appearance,



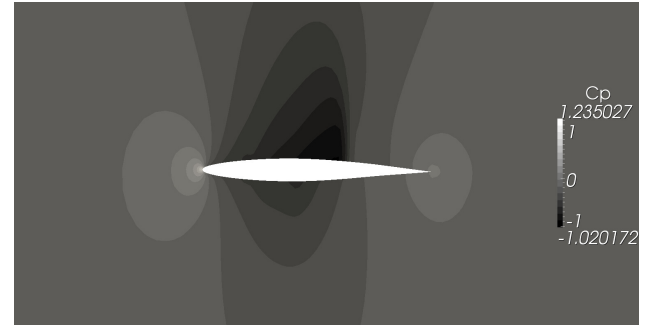
(a) Pitch response.



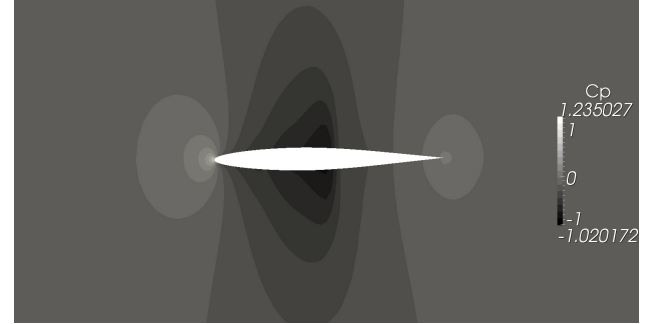
(b) Related control effort.

 Fig. 5 : High fidelity response to off-on control, $V_\infty = 255$, m/s.

applies also after accounting for just the previously used sensor dynamics, even if its 25 [Hz] bandwidth is well in excess of the limit cycle frequency. Such outcomes clearly point out the need of taking into account any significant realization delay from the very inception of a design procedure. Finally, the robustness of the proposed approach is tested in the case where a control surface free-play [19] is present in the control actuation system. A fairly large value is chosen ($\beta_{\text{free-play}} = 0.5$, deg) and the controller described by Table 1 is tested on the system characterized by such a nonlinearity. The obtained results are shown in Fig. 8. As can be noticed, the control law is able to maintain the response bounded, guaranteeing a stable behavior, yet not being able



(a) Rear position of the shock during the limit cycle.



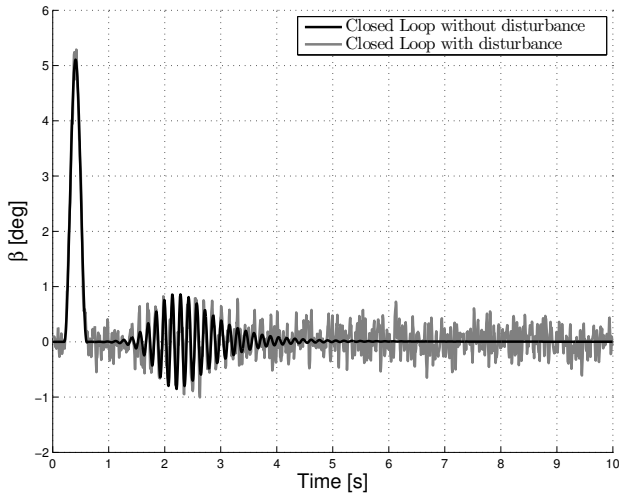
(b) Stabilized position.

Fig. 6 : Various phases during the limit cycle oscillation suppression.

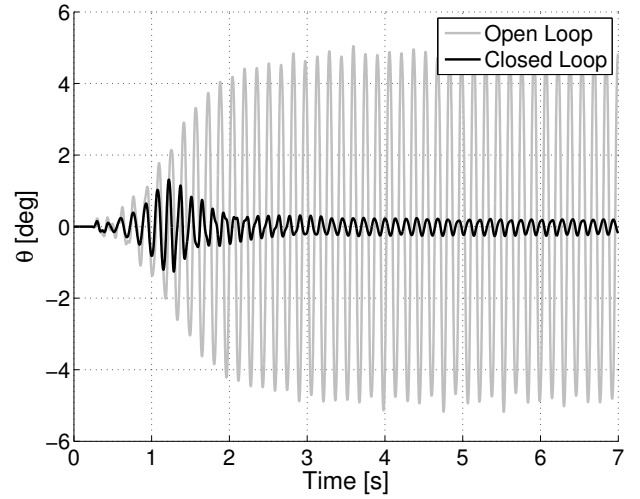
to compensate the presence of the free-play, leading to a residual LCO in the closed loop response.

5 Concluding remarks

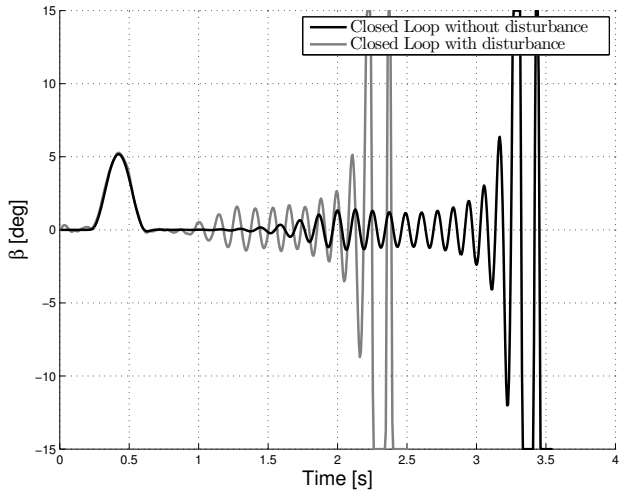
The paper has presented an adaptive approach for the active suppression of a possible nonlinear flutter through a full state Immersion and Invariance (I&I) controller, coupled to a sliding mode observer. The resulting adaptive controller provided fairly robust stabilisation properties against differing flow conditions, sizeable system disturbances, model order and parameters variations. Moreover the importance of embodying appropriate formulations of the dynamics of sensors and actuators has been verified, whereas neglecting them could lead to a loss of robustness, mated to a difficult implementation. Finally, the designed control law has been tested against the possible presence of a free-play nonlinearity in the control surface actuation system. Even if the obtained results are encouraging, it is believed that to fully verify the strength and weaknesses of



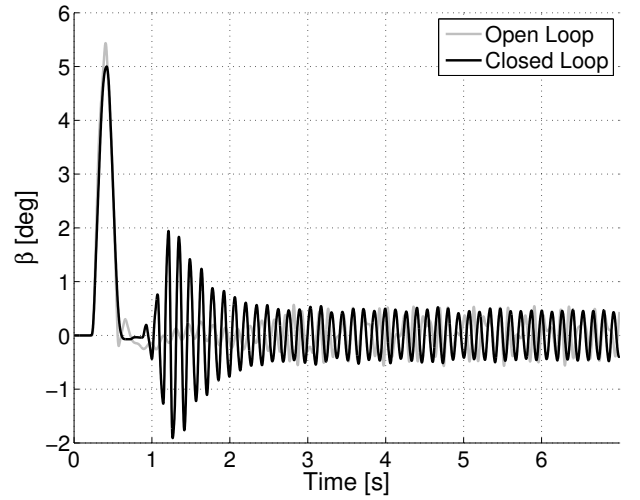
(a) Ideal control surface deflection.



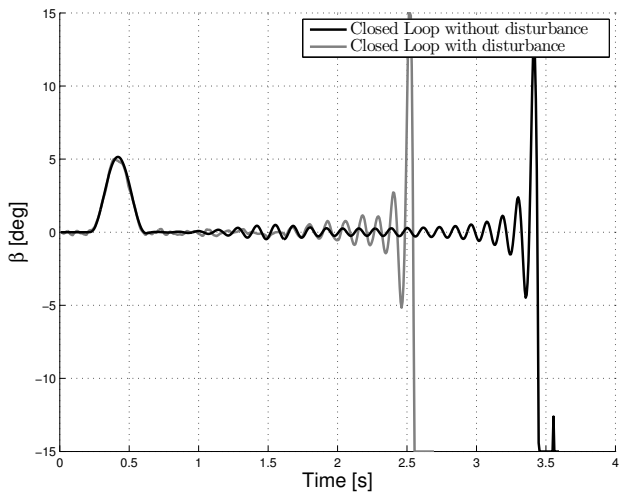
(a) Pitch response.



(b) Ideal design response, after modeling the actuator.



(b) Related control effort.



(c) Ideal design response, after modeling the accelerometers.

Fig. 7 : Effects of omitting sensors and actuator dynamics in the design.

Fig. 8 : Input pulse response of the model with control surface free-play, $V_\infty = 255$, m/s.

a non linear adaptive I&I controller there remains the need of focusing on more complex and realistic applications, e.g. multi-input and deformable free flying aircraft, integrating true design specifications related to stability and response performances.

Copyright Statement

The authors confirm that they, and/or their company or organization, hold copyright on all of the original material included in this paper. The authors also confirm that they have obtained permission, from the copyright holder of any third party material included in this paper, to publish it as part of their paper. The authors confirm that they give per-

mission, or have obtained permission from the copyright holder of this paper, for the publication and distribution of this paper as part of the ICAS 2014 proceedings or as individual off-prints from the proceedings.

References

- [1] S. A. Jacklin. Closing the Certification Gaps in Adaptive Flight Control Software. In *AIAA Guidance, Navigation and Control Conference, Honolulu, AIAA Paper 2008-6988*, 2008.
- [2] K. Becker and J. Vassberg. Numerical Aerodynamics in Transport Aircraft Design. *Notes on Numerical Fluid Mechanics*, 100(1):209–220, 2009.
- [3] V. Mukhopadhyay. Historical Perspective on Analysis and Control of Aeroelastic Responses. *Journal of Guidance, Control and Dynamics*, 26(5):673–684, 2003.
- [4] A. Astolfi, D. Karagiannis, and R. Ortega. *Nonlinear and Adaptive Control with Applications*, pp. 91–114, Chap. 5. Springer, New York, NY, 2008.
- [5] D. Seo and M. R. Akella. High Performance Spacecraft Attitude-Tracking Control Through Attracting Manifold Design. *Journal of Guidance, Control and Dynamics*, 31(4):884–891, 2008.
- [6] D. Seo and M. R. Akella. Non-Certainty Equivalent Adaptive Control for Robot Manipulator Systems. *System and Control Letters*, 58(4):304–308, 2009.
- [7] K. W. Lee and S. N. Singh. Immersion- and Invariance-Based Adaptive Control of a Nonlinear Aeroelastic System. *Journal of Guidance, Control and Dynamics*, 32(4):1100–1110, 2009.
- [8] K.W. Lee and S. N. Singh. Non-Certainty-Equivalent Adaptive Control of a Nonlinear Aeroelastic System. *International Journal of Electronics and Telecommunications*, 56(4):463–471, 2010.
- [9] W. L. Lee and S. N. Singh. Multi-Input Noncertainty-Equivalent Adaptive Control of an Aeroelastic System. *Journal of Guidance, Control and Dynamics*, 33(5):1451–1460, 2010.
- [10] G Romanelli, E. Seriola, and P. Mantegazza. A "Free" Approach to Computational Aeroelasticity. In *48th AIAA Aerospace Sciences Meeting and Exhibit, AIAA Paper 2010-0176, Orlando, FL*, 2010.
- [11] M. Ripepi and P. Mantegazza. Improved Matrix Fraction Approximation of Aerodynamic Transfer Matrices. *AIAA Journal*, 51(5):1156–1173, 2013.
- [12] K.C. Hall, J. Thomas, and E. Dowell. Proper Orthogonal Decomposition Technique for Transonic Unsteady Aerodynamic Flows. *AIAA Journal*, 38(10):1853–1862, 2000.
- [13] D. J. Lucia, P. S. Beran, and W. A. Silva. Reduced-order modeling: new approaches for computational physics. *Progress in Aerospace Sciences*, 40(1-2):51–117, 2004.
- [14] A. Mannarino and P. Mantegazza. Nonlinear aeroelastic reduced order modeling by recurrent neural networks. *Journal of Fluids and Structures*, In press, 2014.
- [15] A. N. Atassi and H. K. Khalil. A Separation Principle for the Stabilization of a Class of Nonlinear Systems. *IEEE Transactions on Automatic Control*, 44(9):1672–1687, 1999.
- [16] S. Drakunov and V. Utkin. Sliding mode observers. tutorial. In *Proceedings of the 34th Conference on Decision and Control, IEEE, New Brunswick, NJ*, pages 3376–3378, 1995.
- [17] J. P. Thomas, E. H. Dowell, and K. C. Hall. Nonlinear inviscid aerodynamic effects on transonic divergence, flutter, and limit-cycle oscillations. *AIAA Journal*, 40(4):638–646, 2002.
- [18] W. Yao and M. Liou. Reduced-order modeling for flutter/LCO using recurrent artificial neural network. In *12th AIAA Aviation Technology, Integration, and Operations (ATIO) Conference and 14th AIAA/ISSM, AIAA Paper 2012-5446, Indianapolis, IN*, 2012.
- [19] D. M. Tang and E. H. Dowell. Computational/experimental aeroelastic study for a horizontal-tail model with free play. *AIAA Journal: devoted to aerospace research and development*, 51(2):341–352, 2013.